Spectroscopic determination of the doping and mobility of terahertz quantum cascade structures

J. Lloyd-Hughes,[a] Y. L. Delley, G. Scalari, M. Fischer, V. Liverini, M. Beck, and J. Faist
Institute for Quantum Electronics, ETH Zurich, 8092 Zurich, Switzerland

(Received 15 September 2009; accepted 17 September 2009; published online 5 November 2009)

Terahertz time-domain spectroscopy is shown to provide a convenient and rapid means to measure the conductivity of individual layers in semiconductor heterostructures such as terahertz quantum cascade lasers. By modeling the complex transmission at terahertz frequencies, the electron density and the in-plane momentum scattering time of the active regions and doped contact layers were determined for both GaAs/AlGaAs and InGaAs/InAlAs epilayers. The measured temperature dependence of the electron scattering rate revealed the significance of impurity and LO phonon scattering. The implications for laser operation at room temperature are discussed by considering the changes in absorption and resonant tunneling current with temperature. © *2009 American Institute of Physics*. [doi:10.1063/1.3247973]

I. INTRODUCTION

Quantum cascade lasers (QCLs) are compact and convenient sources of radiation in the mid-infrared and far-infrared ranges of the electromagnetic spectrum,[1–3] where the optical gain is provided by a semiconductor heterostructure with a tailored electronic bandstructure. In order to optimize the performance of QCLs, it is desirable to know accurately the donor density in the epilayers, both in the active region and in the other layers in the waveguide. Sufficient doping is required to stabilize device current-voltage characteristics without substantial free-carrier absorption. The doping concentration in the active region can also alter the threshold and maximum current density.[4–6] In terahertz QCLs with single-plasmon waveguides, the overlap of the optical mode with the active region is strongly dependent on the thickness and doping of the buried contact layer.[7] Various techniques that allow the doping density to be determined include capacitance-voltage measurements, electrochemical etching, and the Hall effect. However, these methods have the disadvantages of requiring device fabrication and/or working only in a limited temperature range. Another important parameter is the in-plane electron scattering time $\tau_{\perp}$, which alters the free-carrier absorption in the heterostructure and the current due to resonant tunneling.[8]

In this paper, we report the electron density and in-plane momentum scattering rate of the active region and contact layers of terahertz quantum cascade structures, obtained via terahertz time-domain spectroscopy. Transmission measurements were performed at normal incidence to the epilayers, with different layers removed by chemical etching. This approach has the advantage of not requiring any device fabrication, removing the requirement for labor-intensive photolithographic steps. While the electric field for intersubband gain and absorption in QCLs is parallel to the growth direction, here we report the in-plane absorption, which we show gives access to parameters that strongly influence the temperature performance of QCLs.

[a]Electronic mail: james.lloyd-hughes@phys.ethz.ch.

II. TRANSMISSION MEASUREMENTS AND MODEL

Our terahertz time-domain spectrometer used the frequency-doubled output of a 100 fs Er:fiber laser oscillator (1.55 μm, 300 mW, 90 MHz) to generate pulses of terahertz radiation from a biased semi-insulating GaAs photoconductive antenna. Detection was performed using electro-optic sampling with a ZnTe crystal. The experimental setup was similar to that of Ref. 9. For each epilayer, we created four samples by chemical etching in $H_2SO_4:H_2O_2:H_2O$, removing either (i) the whole epilayer, (ii) the top doped layer plus the active region, (iii) just the top contact, or (iv) nothing. The exact thickness removed in each case was measured with a surface profilometer. Samples were held in an optical cryostat at temperatures from 4 to 300 K, and transmission data were obtained taking the reference scan either through sample (i) or through an empty sample holder. The terahertz pulses were linearly polarized in the plane of the quantum wells, and thus are sensitive only to the in-plane electron conductivity (the hole conductivity is substantially lower owing to the larger effective mass of holes, and the *n*-type doping used).

We investigated the transmission of terahertz radiation through four different epilayers: (a) a GaAs/AlGaAs terahertz quantum cascade structure with a step-well design,[10] (b) a modulation-doped GaAs/AlGaAs multiple quantum well (MQW),[11] (c) an InGaAs/AlInAs terahertz QCL (with a four-well resonant phonon design), and (d) a GaAs/AlGaAs modulation-doped two-dimensional electron gas (2DEG). Figure 1 shows the amplitude of the terahertz electric field transmission of heterostructures [Figs. 1(a) and 1(b)], relative to the transmission through the substrate. The transmission (solid lines) through just the bottom doped layer can be seen to reduce substantially at low frequencies, as a result of free-carrier absorption below the plasma frequency, with similar spectra for the MQW and step-well epilayers. The transmission spectra through the active region and bottom contact are also shown. For the MQW structure, the heavy doping reduces the transmission in comparison to that through just the bottom contact. For the step-well structure,

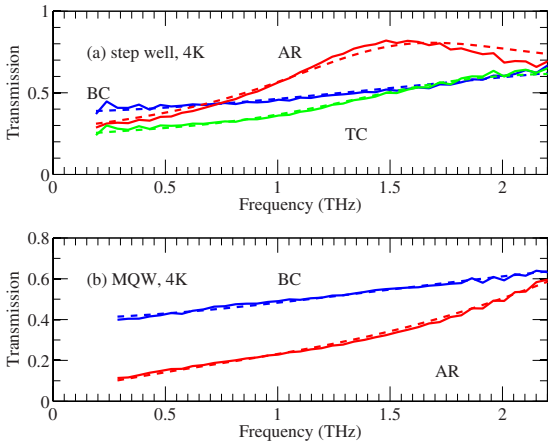

FIG. 1. (Color online) The electric field transmission (relative to the substrate) of terahertz radiation through (a) the step-well sample and (b) the MQW structure, for the bottom contact (BC), the active region (AR) and BC, and the complete epilayer including the top contact (TC). The solid lines are the measured data and the dashed lines are fits to the transmission using the transfer matrix method (see Sec. II). The error in the amplitude of the transmission is 1% at 1.0 THz, increasing to 5% at 2.0 THz.

however, the transmission exhibits a peak around 1.5 THz, where the relative transmission even exceeds that through the bottom contact. This is a result of the Fabry–Pérot etalon (~13.4-μm-thick) created by the bottom contact and the semiconductor/vacuum interface. The InGaAs/AlInAs epilayer [sample (c)] was thinner (~11.8 μm), resulting in a Fabry–Pérot peak at a higher frequency (1.8 THz). The addition of the doped top contact reduces the overall transmission again, and dampens the amplitude of the Fabry–Pérot mode as it acts like a metallic broadband impedance-matching layer.[12]

In order to proceed from this qualitative understanding of the spectra to a quantitative determination of the properties of the epilayers, we employ the transmission matrix method[13] to calculate the complex transmission of each stack of dielectric layers. The Drude–Lorentz dielectric function for a free-electron gas is used for each layer, where the free fit parameters are the carrier density and the in-plane momentum scattering time.[14] This model is a first-order approximation for the response of electrons, as it does not include carrier localization effects. The electrons are assumed to be uniformly distributed throughout the quantum wells of each structure. Literature values were used for the temperature dependence of the high and low frequency dielectric constants and the thermal expansion coefficient. The electron effective mass was taken from cyclotron measurements on similar quantum cascade structures.[15] The transmission lineshapes obtained using this model are shown by the dashed lines in Fig. 1, and accurately fit the measurements, including the Fabry–Pérot resonance of the active region. While the transmission data in Fig. 1 were obtained using a time window to exclude the Fabry–Pérot reflections of the substrate, we can optionally include these data and model to obtain the dielectric function and thickness of the substrate.

The modeled complex conductivity of the layers of the step-well quantum cascade structure are shown in Fig. 2, obtained from the Drude–Lorentz approach and the transmission fitting method outlined above. The conductivity of the active region decreases at higher temperatures [Figs. 2(a) and 2(b)], and the peak of the imaginary part shifts to higher frequencies. The conductivity of the top contact is roughly twice that of the bottom contact [Figs. 2(c) and 2(d)]. It is worth noting that the carrier density primarily alters the scale of the conductivity, while the lifetime changes the frequency of the maximum imaginary part of the conductivity.

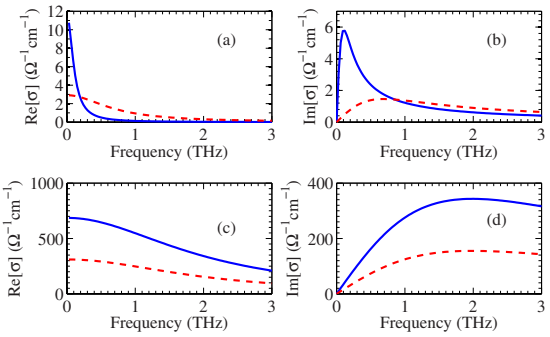

FIG. 2. (Color online) Complex conductivity of regions of the step-well structure extracted from the transmission model. (a) Real and (b) imaginary part of conductivity at 10 K (solid lines, electron density $N=1.9\times10^{15}$ cm^{-3}, lifetime $\tau_\perp=1.5$ ps) and 300 K (dashed lines, $N=3.1\times10^{15}$ cm^{-3}, lifetime $\tau_\perp=0.23$ ps). (c) Real and (d) imaginary part of the conductivity at 10 K for the top (solid lines, $N=2.1\times10^{18}$ cm^{-3}, lifetime $\tau_\perp=0.09$ ps) and bottom (dashed lines, $N=1.0\times10^{18}$ cm^{-3}, lifetime $\tau_\perp=0.09$ ps) heavily doped contacts.

III. ELECTRON DENSITY AND SCATTERING LIFETIME

Using this model, the electron density and in-plane momentum scattering lifetime $\tau_\perp$ for each region of the heterostructure were determined as a function of temperature, as shown in Figs. 3 and 4. The electron density is essentially independent of temperature for both the heavily doped layers ($>1\times10^{18}$ cm^{-3}) and the doped quantum well regions. In the former case no carrier freeze-out is observed as the

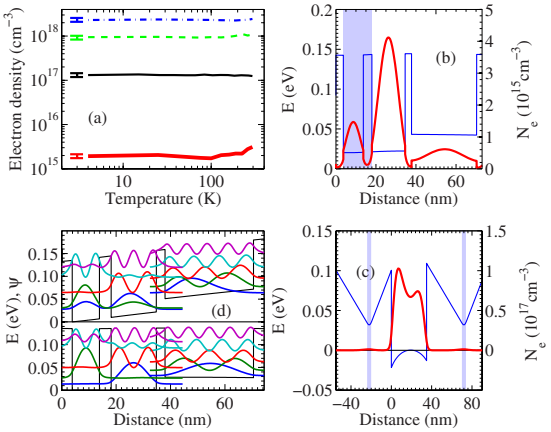

FIG. 3. (Color online) (a) Electron density extracted from the transmission at different temperatures, for the top and bottom contact layers of the step-well structure (dashed-dotted and dashed lines), and for the active region (thick line). The electron density for the wells of the MQW sample is also shown (thin line). The error in the density is 10%, as indicated by the error bars. (b) Potential energy (thin line, left y-axis) and simulated electronic density (thick line, right y-axis) in the step-well sample at 100 K. (c) Same as (b) but for the MQW sample. (d) Bandstructure of step-well structure at 10 K at the design bias (top) and at zero bias (bottom).

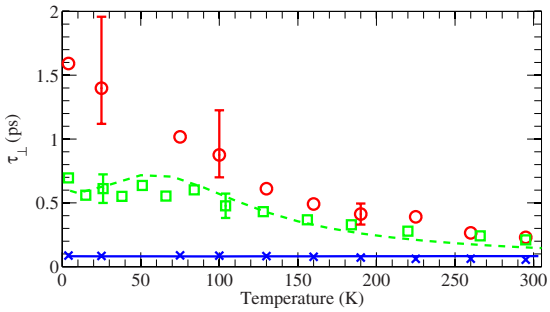

FIG. 4. (Color online) The measured temperature dependence of the in-plane scattering lifetime $\tau_\perp$ is shown for the wells of the MQW sample (squares) and the wells (circles) and top contact (crosses) of the step-well design. The theoretical temperature dependence of $\tau_\perp$ for the top contact (solid line) and MQWs (dashed line) are also shown.

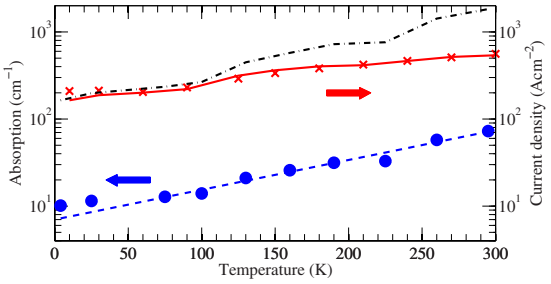

FIG. 5. (Color online) The temperature dependence of the in-plane absorption coefficient α at 3 THz (circles, left axis) and the measured current density at the NDR of a nonlasing ridge of the step-well design (crosses, right axis). The dotted line is a fit $\alpha=\alpha_0 e^{T/T_0}$ with $T_0=110\pm10$ K. The current density due to resonant tunneling is shown calculated from Eq. (1) (solid line) and in the strong coupling regime (dashed-dotted line).

chemical potential remains in the conduction band, while for the wells, the modulation doping scheme employed ensures that the donors are ionized even at low temperature. In order to compare the measured electron density with the nominal values we performed a self-consistent solution to the Schrödinger–Poisson equation for each structure (at zero bias voltage). The conduction band energy and electron density of the GaAs designs are reported in Figs. 3(b) and 3(c) at 100 K. The doped regions are shaded and the electron distribution can be seen to be spatially separated from the dopants in both structures. There is an excellent accord between the electron densities extracted from the experimental data via the transmission model and the simulation. For the step-well sample the measured density is $(2.0\pm0.2)\times10^{15}$ cm^{-3}, while the simulation yields a mean density of 1.4×10^{15} cm^{-3}. In terms of sheet density, the experimental result corresponds to $(1.2\pm0.1)\times10^{10}$ cm^{-2}, and agrees well with that measured independently via the *C-V* technique, $(1.3\pm0.1)\times10^{10}$ cm^{-2}. Similarly, good agreement is obtained for the MQW sample. The measured sheet density of the InGaAs QCL was $(3.9\pm0.4)\times10^{10}$ cm^{-2}, close to the nominal growth value of 4.6×10^{10} cm^{-2}.

In Fig. 3(d), the bandstucture of the step-well design is shown at zero bias (bottom plot) and at the design bias (6.7 kV/cm, top plot). The main difference in the energy levels is that the ground states of the two GaAs quantum wells are degenerate. As the threshold current density[10] is low in this structure ($J_{thr}=100$ A cm^{-2}) the population inversion, roughly $\Delta n=J_{thr}\tau_3/e=0.3\times10^{10}$ cm^{-2} (assuming the upper state lifetime $\tau_3=5$ ps), is small compared with the sheet doping $[(1.3\pm0.1)\times10^{10}$ cm$^{-2}]$. The electron density should therefore be similar for the unbiased and biased cases, with the majority of the electrons in the two GaAs quantum wells, implying that the measured parameters are reasonable for operating QCLs.

The extracted in-plane scattering time $\tau_\perp$ is plotted in Fig. 4 for the wells of the MQW sample and the step-well, and the top contact of the step-well epilayer. The relative error in the lifetime is +40% and −20% when $\tau_\perp>1$ ps because of the low signal-to-noise ratio below 0.3 THz; otherwise it is ±20%. The heavily doped contact has the lowest overall mobility $[\tau_\perp=(80\pm16)$ fs] because of significant electron-impurity scattering. The expected lifetime for this layer was calculated using the Conwell–Weisskopf model of electron-impurity scattering.[16] This model has no free fit parameters, and matches the experimental data well (solid line, Fig. 4). The lifetime of electrons in the MQW sample is higher than that of the doped bulk layer as a result of the modulation doping scheme, which increases the spacing between electrons and impurities. The step-well sample, with a lower sheet doping, has a higher lifetime over the whole temperature range.

We calculated the temperature dependence of $\tau_\perp$ using the energy-dependent electron-impurity and phonon scattering rates for electrons in a quantum well.[17] Using this formalism we find good agreement with the experiment for the MQW structure (dashed line, Fig. 4), where $\tau_\perp$ is dominated by impurity (LO phonon) scattering at low (high) temperature. A satisfactory fit was not obtained for the step-well lifetime, owing to the simplicity of the model, which does not take into account the full subband structure of coupled wells.

Considering now the other structures, we measured $\tau_\perp=(1.0\pm0.5)$ ps at 4 K for our GaAs 2DEG sample with a larger error because the measurement was performed on a single thin layer. At room temperature, the InGaAs QCL had $\tau_\perp=(300\pm60)$ fs, slightly higher than the $\tau_\perp=(230\pm46)$ fs for the GaAs step-well even though the InGaAs structure had a higher doping density. In general the lifetimes determined from terahertz spectroscopy of modulation-doped structures can be much smaller than those derived from transport measurements,[18] which are selective toward small-angle scattering mechanisms.

IV. DISCUSSION

We now relate our results to key parameters that can alter the performance of QCLs. In terahertz QCLs with metal-metal waveguides the mirror losses can be negligible,[7] and the condition for laser action is that the modal gain equals the waveguide's absorption coefficient α_w. Contributions to α_w come from free-carrier absorption in the doped contact layers and metal cladding, and intersubband absorption in the active region. The temperature dependence of the intersubband lifetime should be similar to that of $\tau_\perp$ as both are dominated by phonon scattering at high temperature.[17] In Fig. 5, the in-plane absorption coefficient α of the active

region of the step-well design is shown versus temperature (circles), calculated at the laser frequency (3 THz) using the values of n_s and $\tau_\perp$ extracted from the transmission measurements. α increases exponentially with temperature and a fit of the form $\alpha = \alpha_0 e^{T/T^*}$ yields $T^* = 110 \pm 10$ K. The peak gain in a QCL is proportional to the inverse of the electroluminescence linewidth (dominated by $\tau_\perp$),[3] and will therefore also decrease with temperature, making lasing ever harder to achieve at higher temperature.

Further insights into how changes in $\tau_\perp$ can alter the performance of terahertz QCLs can be obtained by considering the resonant tunneling current density,[8,19] which at the injection resonance is given by

$$J = qn_s \frac{2|\Omega|^2 \tau_\perp}{1 + 4|\Omega|^2 \tau_3 \tau_\perp}. \quad (1)$$

Here, the electron charge and sheet density are q and n_s, the lifetime of the upper laser state is τ_3, and $2\hbar|\Omega|$ is the energy splitting of the injector and upper laser states at resonance. A strong coupling between the injection state and the upper laser state (desirable for laser action) is obtained when $4|\Omega|^2 \tau_3 \tau_\perp \gg 1$. However, at high temperatures, this condition may not be fulfilled as a result of the drop in $\tau_\perp$ and τ_3 from enhanced phonon scattering. We calculated $J(T)$ at resonance using the experimental values of $\tau_\perp$ and n_s for the step-well design, and compared it to the measured current density at the negative differential resistance point (NDR) for a nonlasing ridge. We assumed that τ_3 has the same temperature dependence as $\tau_\perp$. The calculated current density (solid line in Fig. 5) agrees well with the measured J when $\tau_3(T=0) = 3.9$ ps and $2\hbar|\Omega| = 1.2$ meV. With these values, which are typical for terahertz QCLs, the resonant tunneling current starts to deviate from that in the strong coupling regime ($J = qn_s/2\tau_3$, dashed-dotted line in Fig. 5) at around 130 K, due to the reduction in τ_3 and $\tau_\perp$. This implies that the injection efficiency into the upper state is reduced at higher lattice temperatures,[19] which reduces the maximum achievable gain.

V. CONCLUSION

In summary, we have demonstrated that terahertz time-domain spectroscopy can determine accurately the temperature dependent electron density and scattering time of complex semiconductor heterostructures such as terahertz QCLs. The influence of $\tau_\perp$ on the tunneling current and absorption has implications for the design of terahertz QCLs operating above cryogenic temperatures.

ACKNOWLEDGMENTS

The authors would like to thank M.I. Amanti for technical assistance. This work was supported by the Swiss National Science Foundation and the Marie Curie Training Network POISE.

[1] J. Faist, F. Capasso, D. L. Sivco, C. Sirtori, A. L. Hutchinson, and A. Y. Cho, Science **264**, 553 (1994).
[2] R. Kohler, A. Tredicucci, F. Beltram, H. E. Beere, E. H. Linfield, A. G. Davies, D. A. Ritchie, R. C. Iotti, and F. Rossi, Nature (London) **417**, 156 (2002).
[3] G. Scalari, C. Walther, M. Fischer, R. Terazzi, H. Beere, D. Ritchie, and J. Faist, Laser Photonics Rev. **3**, 45 (2009).
[4] M. Giehler, R. Hey, H. Kostial, S. Cronenberg, T. Ohtsuka, L. Schrottke, and H. T. Grahn, Appl. Phys. Lett. **82**, 671 (2003).
[5] H. C. Liu, M. Wachter, D. Ban, Z. R. Wasilewski, M. Buchanan, G. C. Aers, J. C. Cao, S. L. Feng, B. S. Williams, and Q. Hu, Appl. Phys. Lett. **87**, 141102 (2005).
[6] A. Benz, G. Fasching, A. M. Andrews, M. Martl, K. Unterrainer, T. Roch, W. Schrenk, S. Golka, and G. Strasser, Appl. Phys. Lett. **90**, 101107 (2007).
[7] S. Kohen, B. S. Williams, and Q. Hu, J. Appl. Phys. **97**, 053106 (2005).
[8] R. F. Kazarinov and R. A. Suris, Sov. Phys. Semicond. **5**, 707 (1971).
[9] M. B. Johnston, L. M. Herz, A. L. T. Khan, A. Kohler, A. G. Davies, and E. H. Linfield, Chem. Phys. Lett. **377**, 256 (2003).
[10] G. Scalari, M. I. Amanti, M. Fischer, R. Terazzi, C. Walther, M. Beck, and J. Faist, Appl. Phys. Lett. **94**, 041114 (2009).
[11] The MQW structure was (from the top of the structure, with layer thicknesses in nanometers): **5.0**; 85×(35.0/**4.0**/20.0/35.0); 35.0; **300**. Here, the barrier layers (underlined) are $Al_{0.15}Ga_{0.85}As$ and the wells are GaAs. Doped layers are in bold; the top and bottom contact were silicon-doped at 2×10^{18} cm^{-3}, while the modulation doping in the 4 nm $Al_{0.15}Ga_{0.85}As$ region was 1×10^{18} cm^{-3}.
[12] J. Kroll, J. Darmo, and K. Unterrainer, Opt. Express **15**, 6552 (2007).
[13] M. Born and E. Wolf, *Principles of Optics*, 7th ed. (Cambridge University Press, Cambridge, 2007).
[14] The lifetime of the heavily doped contacts was found to be weakly frequency dependent, reducing by a factor of two across our spectral range. This frequency dependence was included in the data presented here, and will be discussed in a future publication.
[15] J. Lloyd-Hughes, H. E. Beere, D. A. Ritchie, and M. B. Johnston, Phys. Rev. B **77**, 125322 (2008).
[16] P. Y. Yu and M. Cardona, *Fundamentals of Semiconductors*, 3rd ed. (Springer, New York, 2003).
[17] T. Unuma, M. Yoshita, T. Noda, H. Sakaki, and H. Akiyama, J. Appl. Phys. **93**, 1586 (2003).
[18] N. A. Kabir, Y. Yoon, J. R. Knab, J. Y. Chen, A. G. Markelz, J. L. Reno, Y. Sadofyev, S. Johnson, Y. H. Zhang, and J. P. Bird, Appl. Phys. Lett. **89**, 132109 (2006).
[19] C. Sirtori, F. Capasso, J. Faist, A. L. Hutchinson, D. L. Sivco, and A. Y. Cho, IEEE J. Quantum Electron. **34**, 1722 (1998).